

www.acsami.org Research Article

Toehold-Mediated Shape Transition of Nucleic Acid Nanoparticles

Jordan Hartung, Nathan McCann, Erwin Doe, Hannah Hayth, Kheiria Benkato, M. Brittany Johnson, Mathias Viard, Kirill A. Afonin,* and Emil F. Khisamutdinov*



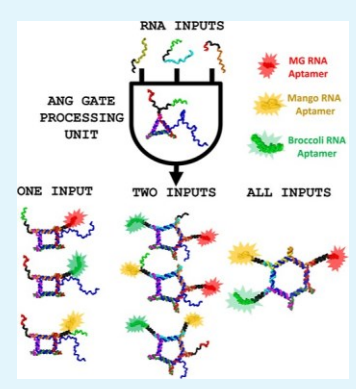
ACCESS

III Metrics & More

Article Recommendations

Supporting Information

ABSTRACT: We introduce a toehold-mediated strand displacement strategy for regulated shape-switching of nucleic acid nanoparticles (NANPs) enabling their sequential transformation from triangular to hexagonal architectures at isothermal conditions. The successful shape transitions were confirmed by electrophoretic mobility shift assays, atomic force microscopy, and dynamic light scattering. Furthermore, implementation of split fluorogenic aptamers allowed for monitoring the individual transitions in real time. Three distinct RNA aptamers malachite green (MG), broccoli, and mango were embedded within NANPs as reporter domains to confirm shape transitions. While MG "lights up" within the square, pentagonal, and hexagonal constructs, the broccoli is activated only upon formation of pentagon and hexagon NANPs, and mango reports only the presence of hexagons. Moreover, the designed RNA fluorogenic platform can be employed to construct a logic gate that performs an AND operation with three single-stranded RNA inputs by implementing a non-sequential polygon transformation approach. Importantly, the polygonal scaffolds displayed promising potential as drug delivery agents and biosensors. All



polygons exhibited effective cellular internalization followed by specific gene silencing when decorated with fluorophores and RNAi inducers. This work offers a new perspective for the design of toehold-mediated shape-switching nanodevices to activate different light-up aptamers for the development of biosensors, logic gates, and therapeutic devices in the nucleic acid nanotechnology.

KEYWORDS: NANPs, RNA nanotechnology, fluorogenic aptamers, RNAi, immunorecognitioin

INTRODUCTION

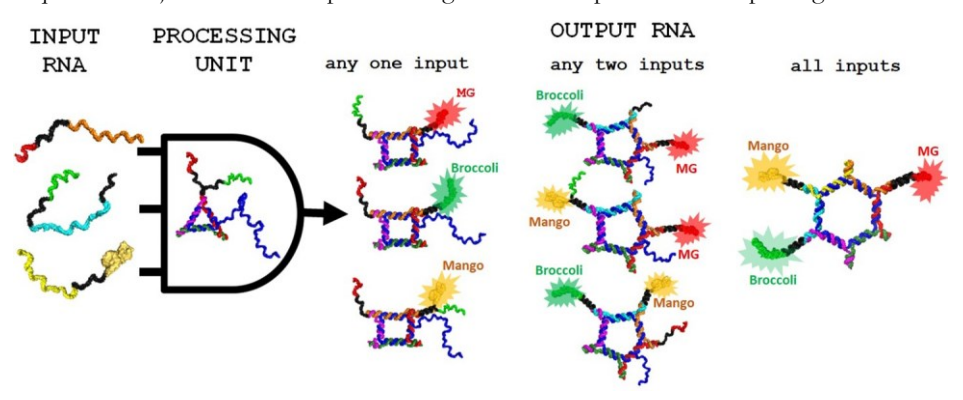
Nanoparticles can be fabricated from various materials ranging from metal atoms (e.g., gold, silver, and iron oxide nanoparticles),1-3 lipid-based materials (e.g., micelles),4 and amino acids (e.g., antibodies and vaccines)⁵⁻⁷ to nucleic acids (e.g., nanostructures made of DNA or RNA) or their chemical analogues.^{8,9} While all these nanomaterials were shown to be effective in synthesis and self-assembly of functional nanoscalesized objects, nucleic acids offer multiple unique advantages. 10-12 The ability of nucleic acids, in particular RNA, to form both canonical (cis-Watson-Crick) and non-canonical base pairs^{13,14} gives rise to a library of structural motifs with a myriad of architectural differences. 15-17 This library is often viewed as modular building blocks to fabricate nucleic acid nanoparticles (NANPs) and nanoscale DNA assemblies in a controlled and pre-programmed fashion.¹⁸⁻²⁴ In addition, the secondary structures of both DNA and RNA can be predicted with high level of accuracy, thus opening possibilities to generate modular NANPs with defined thermodynamic properties and the ability to dynamically respond to the external stimuli.²⁵⁻³¹ The intrinsic properties of nucleic acids to form non-covalent interactions with small molecules, metal ions, polypeptides, other nucleic acids, and large proteins enable the possibility to fabricate sophisticated nanodevices using DNA and RNA as building materials.^{32–34} These unique features expand the possibility of NANPs to serve as highly programmable materials, suitable for applications in synthetic biology, biotechnology, and biosensing.

In the past two decades, a wide range of in silico designed dynamic nucleic acid assemblies have been shown to respond to various ligands including single-stranded oligodeoxynucleotides (ssODNs).35-37 Particularly attractive are studies focused on DNA toehold technologies developed by Yurke and colleagues. 38,39 In the toehold-mediated strand displacement approach, the invading ssODNs bind toehold domains (a single-stranded overhanging region of a duplex DNA) hybridized with a substrate and a protector strand. This binding facilitates the strand displacement through branch migration, releasing the protector strand. In their original work,39 Yurke and co-workers constructed effective DNA molecular tweezers from three strands which can be opened and closed repeatedly by cycling additional auxiliary strand or a "fuel" DNA. As a result of each cycle, a waste product in the form of DNA duplex was produced. Such DNA strand exchange processes have recently been introduced as a major

Received: February 6, 2023 Accepted: May 8, 2023



Scheme 1. Shape Switching of Nucleic Acid Polygonal Nanoparticles Is Achieved by Utilizing Toehold-Mediated Strand Displacement Technique in Conjunction with Split Fluorogenic RNA Aptamers as Reporting Modules



technique for DNA nanofabrication, machinery, computation, and biosensing in order to design autonomous walkers, ⁴⁰ logic robot, ⁴¹ molecular devices and automata, ^{42,43} and other structures that mimic biological processes and can be used in molecular diagnostics. ⁴⁴ Therefore, the dynamic nucleic acid nanotechnology provides a practical method for synthetic biology through the programmable structural transformation of biologically relevant biopolymers. ^{45,46}

A novel design approach to fabricate highly dynamic NANPs is imperative for the fields of RNA and DNA nanotechnology in order to improve the communication of functional systems with one another or external stimuli. Besides DNA-exclusive systems, the structural and functional properties of natural and artificial RNAs were applied to address specific questions by engineering nanodevices that can interact with intracellular components.^{26,29} Previously reported design principles demonstrated conditional activation of gene silencing in diseased cells in vitro and in vivo using a dynamic RNA and RNA – DNA hybrid approach.^{29,31} More recently, Halman et al. introduced a new concept utilizing functionally interdependent and fully complementary cognate NANPs.²⁶ In this approach, the intracellular presence of two cognate NANPs triggers the physical interaction between designed nanoparticles initiating isothermal shape change which in turn, activates multiple functionalities and biological pathways. It is also important to note that the programmable dynamic nature of RNA complexes is actively used to generate nanodevices possessing Boolean functions. In our previous work, we demonstrated a unique design approach to fabricate various logic gates (elementary building block for digital circuits) utilizing properties of fluorogenic RNA.47 The simple logic gates including AND, NAND, OR, and NOR as well as combinatorial half-adder circuits made of AND and XOR gates were shown to respond in the presence or absence of corresponding single-stranded DNA strands. The development of novel dynamic NANP platforms demands advancements in the robust visualization and tracking techniques that often require nanoparticles to be biocompatible.

The fluorogenic RNA aptamers, also known as "light-up" aptamers, activate small fluorophore molecules upon binding. ^{48,49} These reporters have shown some advantages over other imaging techniques such as FRET, FISH, and molecular beacons. ^{50,51} While the latest methods are limited to only exogenously introduced NANPs, the fluorescent dyes must be covalently linked to either the 5′- or 3′-end of nucleic acids, and the light-up RNA aptamers offer excellent real-time

imaging that is label-free, protein-free, has a high signal-tonoise ratio, and possess modularity for simple sequence incorporation and tagging. ^{28,52–55} This opens endless possibilities to program functional NANPs and nucleic acid nanodevices for logical operation in vitro and in vivo. ^{56–59}

In this project, we took advantage of a recent progress made in the nucleic acid nanotechnology field, specifically, in the areas of split fluorescent RNA aptamers and toehold-mediated DNA strand displacement^{28,60} techniques³⁹ to design and experimentally validate multi-color shape switching of NANPs in triangular, square, pentagonal, and hexagonal configurations (Scheme 1). Furthermore, the in vitro data demonstrate excellent internalization of all tested shapes and the ability of RNA interference to effectively silence expression of target genes. This system can be potentially implemented to monitor, in real time, the formation of reconfigurable NANPss as a biosensor to advance emerging field of the nucleic acid nanotechnology and synthetic biology.

RESULTS

Design of Oligonucleotide Responsive DNA Polygons **Enabling Shape Transformation.** The original design and sequence compositions of the core polygonal NANPs were adopted from our previous reports. 12,61,62 The major design principle behind the shape transition among polygons relies on the toehold-mediated strand displacement approach using carefully selected invader DNA or RNA single-stranded sequences. Figure 1A includes a schematic that displays the 2D structures of DNA polygons and the principle for the shape transitions. The sequences and predicted secondary structures are listed in the Supporting Information section in Table S1 and Figure S1. The DNA triangle strands T1 (colored in RED) and T3 (colored in GREEN) were extended at 3'-end and 5'end, respectively, with the addition of 10 nucleotides (nt.) ssDNA overhangs or toehold regions. The DNA leading strand (central strand within the triangular complex, in BLACK color) was designed to serve as a fuel molecule. This long auxiliary DNA contains complementary regions to the sides of all corresponding square (tetragonal), pentagonal, and hexagonal geometries. The addition of invading S4 DNA (colored in brown) containing complementary 10 nt. sequences to the 3'-end overhang toeholds induces T3 strand displacement, resulting in reassociation of this strand to a square complex. As the toehold regions play a key role in facilitating strand displacement, the length of the toehold was chosen to be 10 nt., which generally satisfies the criterion to

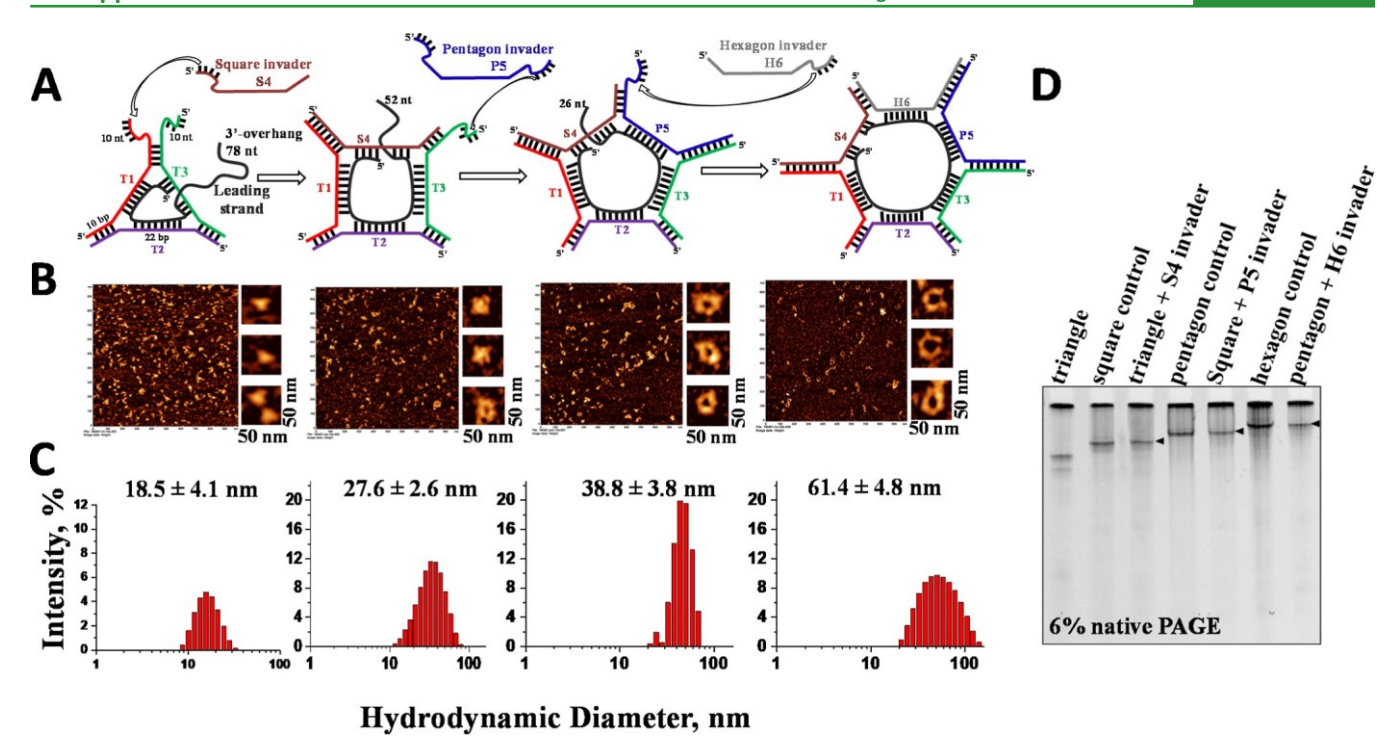


Figure 1. Toehold-mediated DNA shape transition design and validation. (A) Schematic illustration of the sequential shape transformation from triangle to hexagon upon addition of invader strands. (B) Atomic microscopy images of the resulted polygonal nanoparticles demonstrating distinct shapes. (C) Average hydrodynamic diameters of polygons measured in solution by dynamic light scattering; errors indicate standard deviations calculated using triplicate measurements. (D) Native PAGE analysis of the fractions (pointed by arrows) taken after addition of corresponding invader strands to confirm complexation. The fractions run together with annealed control polygons.

thermodynamically enhance the energy difference between products and reactants (products possess more negative freeenergy change).63 The transformation from square to pentagon was facilitated in a similar manner, the invading DNA P5 strand (blue) designed to trigger dissociation of the duplex within the vertex formed between S4 and T3 strands of the square. The P5 strand is designed to carry dual purpose: first, it enables hybridization with the T3 strand and thus induces a conformational change from square to pentagon, and second, it provides a toehold module at its 5'-end to subsequently facilitate transformation from the pentagon to a hexagon in the following step. The addition of the DNA H6 (gray) invading strand completes the transformation process from pentagon to hexagon. Upon formation of the hexagonal nanostructure, the DNA leading or fuel strand is in a fully hybridized form with corresponding invading strands. The secondary structures of the corresponding polygonal complexes were thoroughly analyzed by NUPACK.64

Confirmation of the Shape Transition Using AFM, DLS, and Electrophoretic Mobility Shift Assays (EMSAs). The shapes of the individual NANP polygons were first confirmed by atomic force microscopy, as shown in Figure 1B. Prior to AFM analysis, individual polygons were assembled in one-pot at equimolar concentrations of individual strands and purified using non-denaturing PAGE. The resulting images confirmed the shapes of the corresponding triangle, square, pentagon, and hexagonal DNA polygons. The average dimensions of the NANPs were found to consistently increase from triangular to hexagonal DNA polygons, as demonstrated in the magnified area of the total field AFM surface. Although AFM images provide undisputable information about the geometric topology of the 2D nanoobjects, the technique is

limited to identify the actual dimensions of the NANPs due to the several factors including imaging in air, sharpness of AFM tip, and image deconvolution process. 65,66 We, therefore, further addressed the question regarding the NANP size by performing DLS analysis in an aqueous solution. Assembled DNA complexes $0.5~\mu\text{M}$ in $100~\mu\text{L}$ were directly subjected to DLS measurements without purification. The calculated average hydrodynamic diameters were found to be 18.5, 27.6, 38.8, and 61.4 nm for DNA triangle, square, pentagon, and hexagon, respectively, Figure 1C. The data are in general agreement with nanoparticle dimension approximated by a microscopy technique.

To determine whether the individual NANP shapes can transition from one form to another upon addition of the corresponding invader strand, we performed sequential addition of the invading strand at a 1:1 stoichiometric ratio to the triangular nanoparticle. The subsequent shape transition was monitored by means of gel electrophoresis Figure 1D. We first assembled DNA triangle NANPs at 1 µM from corresponding individual strands (DNA T1, T2, T3, and leading) in TMS buffer at pH = 8.0. The self-assembly efficiency of the DNA triangular shape formation was calculated to be $72 \pm 5\%$ using quantification analysis by ImageJ software.⁶⁷ DNA S4 strand was added to the triangular nanocomplex, and the mixture was left to equilibrate at 37 °C for ~30 min to allow the strand displacement reaction to complete. After taking an aliquot for gel analysis, the DNA P5 strand was added, and the reaction was allowed to incubate for additional 30 min. The same procedure was repeated with the final DNA strand H6. The mobility shift analysis performed using native 6% PAGE shows distinct bands for the triangle + S4 invader sample having an electrophoretic distance identical

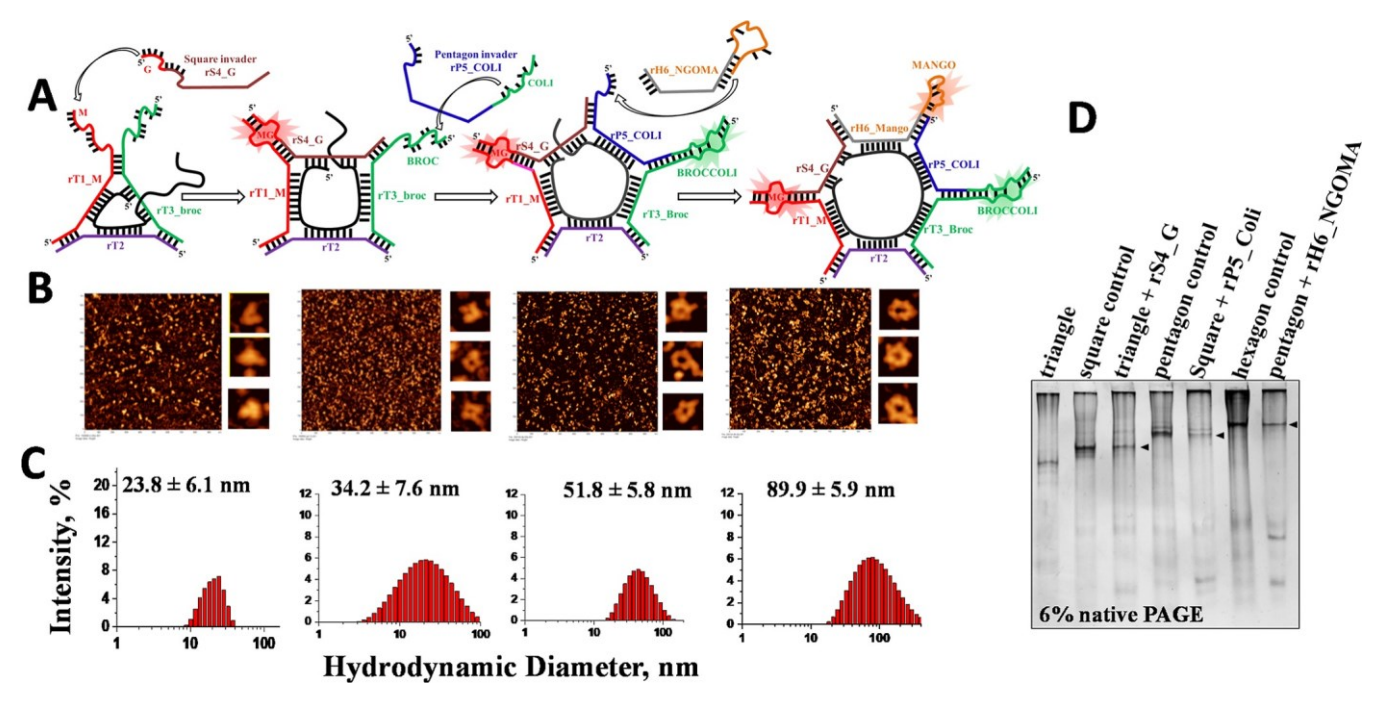


Figure 2. Toehold-mediated RNA polygons harboring MG, broccoli, and mango fluorogenic RNA reporters. (A) Schematic diagram of polygonal shape transition containing split fluorescence aptamers whose shape transitions and fluorescence are influenced by invading strands. (B) AFM images of the RNA polygonal nanolattices (including magnified view) with distinct polygonal shapes. (C) DLS analysis of solution structures of RNA polygons showing average hydrodynamic diameters, and an error represents standard deviation of the mean obtained from at least three independent measurements. (D) Native PAGE analysis of RNA complexes pointed by arrows taken after addition of corresponding RNA invading strands confirming formation of polygons. The one-pot self-assembled polygons were used as migration controls.

to the control square particle. Similarly, distinct bands are obtained for the square +P5 invader and pentagon +H6 invader samples which co-migrate with corresponding pentagon and hexagon control lanes (Figure 1D). The data obtained by this gel shift assay indicate successful sequential transition of the DNA NANPs from triangle to square to pentagon and to hexagon. The presence of 10 nt toehold ssDNA regions is found to be critical for the transition to occur at an isothermal temperature, the control experiment without 10 nt ss region did not induce the transition (data not shown). We next performed a calculation of the DNA polygonal transition yield from one nanoparticle to another using the ImageJ gel shift quantification approach. The percentage yields for such isothermal sequential transition were found to be 68.1, 61.5, and 68.8% for square, pentagonal, and hexagonal DNA configurations, respectively. This demonstrates a moderate result compared to a typical toehold-mediated strand displacement.68,69

Design and Validation of RNA Complexes Enabling the Report of Shape Transition by Emitting a Distinct Fluorescence Signal. The development of novel bioimaging tools enabling visualization and quantification of biochemical and molecular events temporally or spatially within a cellular context is exceedingly important in translational medicine and in basic biology. Molecular imaging is rapidly emerging as an interdisciplinary subject and has been applied widely to study different molecular events including gene expression, molecular trafficking/localization and molecular interactions. Therefore, based on the DNA shape switching conceptual design, we next implemented a split fluorogenic aptamer approach,²⁸ enabling detection of transitions based on the distinct fluorescence output signals of malachite green (MG), broccoli, and mango RNA aptamers. In this approach, the functional RNA aptamers,

possessing a hairpin conformation, are bifurcated into two individual strands diminishing their ability to bind a corresponding fluorogen dye molecule. The fluorescence activation requires hybridization of both strands to reform the binding pocket.

The core RNA sequences of the polygonal geometries were identical to the cognate DNA molecules. The toehold regions were extended with corresponding RNA aptamer sequences (Figure 2A and Supporting Information Figure S2). The triangular nano-construct contained a partial sequence of the MG RNA aptamer rT1_M (red-colored strand) and broccoli aptamer rT3_broc (green-colored strand) (Figure 2A). The addition of the square invader RNA strand, rS4_G, causes hybridization of MG RNA aptamer strands into a functional state and further displacement of the rT3_broc strand, resulting in the nanostructure shape reconfiguration from triangular to square geometry. In a similar fashion, the addition of the pentagon invader RNA containing the complementary half of the broccoli RNA aptamer, rP5_COLI, results in the formation of a functional broccoli RNA reporter structure and reassembly of the square configuration to pentagonal. For the final step, the presence of the Hexagon invader RNA strand transforms the pentagon to the corresponding hexagon and triggers fluorescence due to the correct folding of the mango RNA aptamer.⁵⁶ The mango RNA aptamer contains TO1biotin-binding domain at the loop region, formed by three stacked G-quadruplexes, of the hairpin secondary structure, whereas both MG and broccoli RNA aptamer-binding sites are localized to the helical stems of the hairpins. Due to its unique structural features, the splitting mango RNA aptamer would require significant sequence optimization and laborious experimental selection to achieve the adequate fluorescence output. Instead, the structure of the functional mango RNA

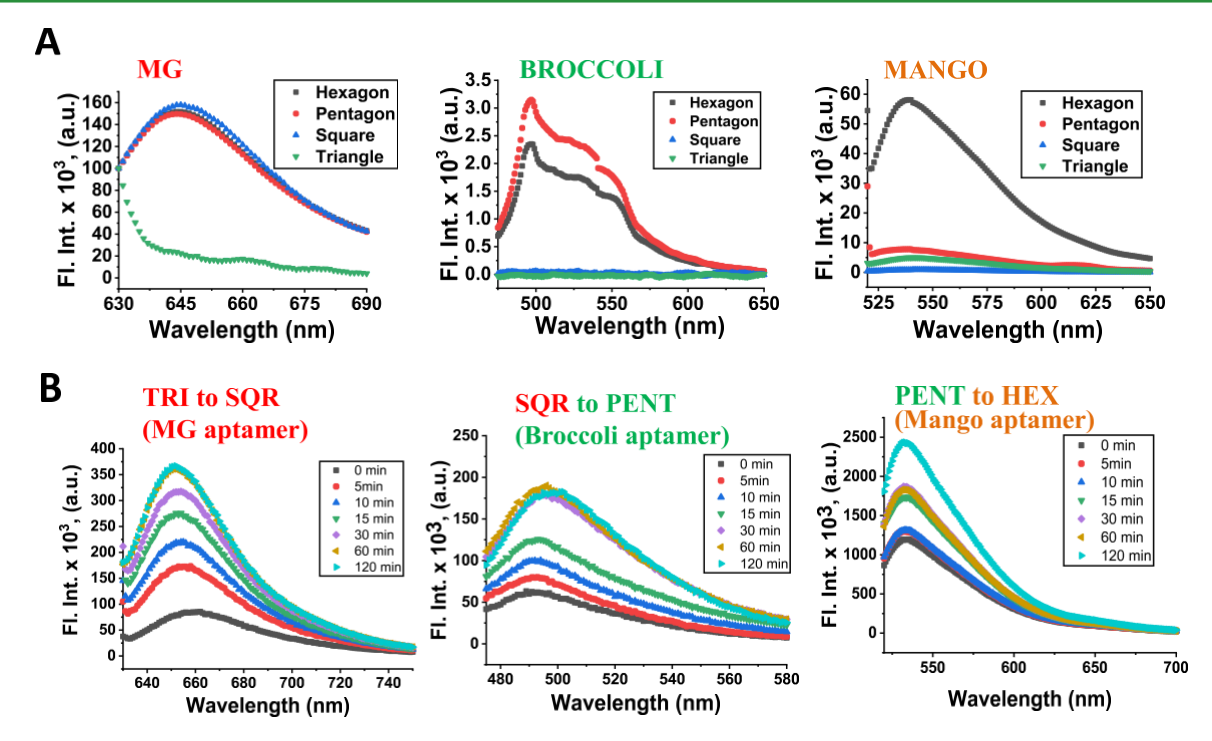


Figure 3. Fluorescence emission spectra of polygonal RNA complexes demonstrating formation of RNA aptamer modules only when a specific polygonal geometry is present. (A) Steady-state emissions captured from each polygon with individual excitation wavelength (λ_{exc}) corresponding to RNA aptamers, MG binding aptamer λ_{exc} = 615 nm, broccoli aptamer λ_{exc} = 475 nm, and mango aptamer λ_{exc} = 510 nm. (B) Time-dependent fluorescence intensities recorded at 37 °C for the transition from the triangle to square in the presence of rS4_G, from square to pentagon in the presence of rP5_Coli, and from pentagon to hexagon upon addition of rH6_Ngoma.

aptamer was inhibited by introducing a competitive sequence region within the rH6_NGOMA strand, pairing with the 3'-end of the mango nucleotides responsible for the correct folding, as illustrated in Supporting Information Figure S3. Upon interaction with the 5'-end single-stranded region of the rP5_coli, the rH6_NGOMA (non-functional state) refolds into a functional state rH6_MANGO. As a result, monitoring the hexagonal complex formation can be performed by observing fluorescence of the mango RNA aptamer.

It is important to note that the shape transition did not yield significant results for both DNA and RNA polygons when experiments were conducted at ambient temperature (Supporting Information Figures S4 and S5). These results suggest that nucleic acid strand displacement reactions tend to occur more efficiently at higher temperatures presumably due to increased thermal energy and faster molecular motion, which can facilitate the necessary base-pairing interactions and reduce kinetic barriers. Given the observed temperature-dependent effects, we have raised the question whether the RNA hexagonal NANPs can be assembled under isothermal conditions (e.g., during transcription). This, in turn, would facilitate the application of the designed RNA polygon switches in the intracellular environments. A co-transcription assay was performed according to previously published protocol by Afonin et al.⁷⁰ The crude RNA product obtained during the in vitro transcription was analyzed by both agarose gel electrophoresis and fluorescence assay, as shown in Supporting Information Figures S5 and S6. The co-transcriptional RNA assemblies displayed intense fluorescence signals characteristic to corresponding RNA aptamers and resulted in a clearly distinguishable band on the agarose gel that co-migrated with the control RNA hexagons. This provides compelling evidence

that the RNA hexagonal NANPs can effectively assemble under isothermal conditions.

AFM and DLS Confirm the RNA Polygonal Shape. AFM images of the purified RNA fractions confirmed predicted polygonal shape configurations, as demonstrated in Figure 2B. The distinct geometrical forms of the triangles, squares, pentagons, and hexagons were found on the mica surface scanned by AFM in air. The DLS data obtained for the individual polygonal fractions provide further evidence of the size increase from triangle to hexagon (Figure 2C). The aqueous solution of the RNA polygonal NANPs was found to be highly heterogeneous by both DLS and AMF methods, the dimension of the RNA complexes surprisingly span from 23.8 nm for triangles and up to 89.9 nm for the hexagons. This large size distribution is presumably due to the additional nucleotide extension to the polygonal vertices containing RNA aptamer regions. Such long sticky ends influence the movement of the RNA nanoparticles in solution and since DLS averages the dimension of the particles depending on their movement,71 this can explain why a large size distribution was observed. This conclusion can be further supported by the fact that DNA polygons, having shorter single-stranded regions, are relatively more homogeneous compared to the RNA polygonal constructs.

The sequential transition of polygonal nano-scaffolds upon addition of the invader strands was further confirmed by EMSA. The transition protocol was conducted similar to the DNA polygon transitions as described above. In this experiment, an equivalent amount of the square invader strand was added to the annealed 1 μ M triangular RNA NANPs, and the resulting mixture was incubated at 37 °C for 30 min (an aliquot was taken for analysis). This process was repeated with pentagon invaders and finally hexagon invaders containing the

mango RNA aptamers. The resulting RNA fractions were evaluated by electrophoretic mobility assay (Figure 2D). The bands indicated by arrows correspond to the fractions of the polygons after transformation.

Control RNA NANPs, where individual strands were annealed, were co-run with the reaction products to calculate the yield of the shape transition. The calculated yields were found to be 46.3, 36.8, and 28.6% for the triangle to square, square to pentagon, and pentagon to hexagon shape transformations, respectively. Notably, the interaction of the invaders with their corresponding RNA complexes induced the refolding of the target polygon conformation. For example, incubation of RNA triangle with rS4_G produced not only a square NP but also other high-molecular-weight RNA complexes trapped at the beginning of the gel well, with no detectable fractions of triangles.

Fluorogenic RNA Aptamers Report the Presence of Distinct Polygonal Conformation. A fluorescence assay was performed in solution next to investigate the fluorescence reportability of polygonal nanostructures following shape transformation. The emission spectra were measured for the individual RNA polygons and upon their transition when invader strands were added.

A steady-state fluorescence spectrum of the MG RNA aptamer that "light-ups" in the presence of the square, pentagon, or hexagon configurations is shown in Figure 3A. The broccoli RNA aptamer exhibits strong emission signals when the pentagonal and hexagonal polygons are formed, whereas the mango RNA aptamer becomes functional only with formation of the hexagon RNA nanoparticles. The fluorescence spectra were measured in TMS buffer pH = 8.0 at ambient conditions in the presence of exceeding concentrations of three dyes MG, DFHBI, and TO1-biotin using individual fluorophore excitation wavelength, as described in the Materials and Methods section.

Additionally, real-time monitoring was conducted to observe the sequential formation of fluorogenic RNA polygons. Figure 3B displays the emission maxima wavelength of individual polygons over time after the corresponding invading strands were added. The formation of squares was detected using the MG-binding RNA aptamer, the formation of pentagons was monitored using the broccoli aptamer, and the formation of hexagons was measured using the mango RNA aptamer. The experiments were conducted at 37 °C, and, in general, 30 min of incubation was sufficient for all aptamers to produce strong fluorescence emissions, indicating that the shape configuration transitions occur in a similar time frame.

Importantly, the RNA shape reconfiguration can be monitored using a single excitation wavelength centered at 420 nm and recording emission spectra from 475 to 700 nm. An example of such a spectrum is shown in Supporting Information Figure S7. The assembled triangular RNA nanoparticle exhibits no distinct fluorescence maxima. However, upon the addition of rS4_G, the MG signal becomes strong at 650 nm. Further sequential addition of rP5_Coli and rH6_Ngoma strands produces corresponding maxima of broccoli and mango aptamers at 500 and 530 nm, respectively. Therefore, for a given set of four polygonal mixtures, it is possible to identify the configuration of the specific polygonal shape based on the fluorescence outputs, as exemplified in Table 1. Such a system holds a great promise to further exploit the potential of polygonal reporters as an arithmetic tool for

Table 1. Fluorescence-Based Polygon Shape Identification

fluorogenic reporter	triangle	square	pentagon	hexagon
malachite green	OFF	ON	ON	ON
broccoli	OFF	OFF	ON	ON
mango	OFF	OFF	OFF	ON
U				

molecular programming to develop well-regulated molecular devices and biosensors based on a three-input logic system.

Fluorescent Assessment of Non-sequential Nucleic Acid Shape Formations Enabling Design of a Three-**Input AND Logic Gate.** The designed nucleic acid sequences were found to be highly versatile, as demonstrated by their ability to self-assemble into various fluorogenic polygons (Supporting Information Figures S8 and S9). In addition to the sequential shape reconfiguration design approach, we also tested the toehold-induced assembly of squares, pentagons, and a hexagon using a combination of different oligonucleotides. Specifically, annealed triangular NANPs were incubated with individual oligonucleotides, combinations of oligonucleotides, and all oligonucleotides together at 37 °C, as shown in Figure 4. This approach allowed us to explore the full potential of the designed nucleic acid sequences in creating a diverse range of polygonal NANPs with different shapes and emission properties.

Figure 4A illustrates schematic diagrams of secondary structures for all possible combinations of polygons numbered from 1 to 7. In order to investigate the fluorescence reportability of the resulting polygons upon addition of invading strands, fluorescence measurements were performed. Figure 4B shows the fluorescence intensities for broccoli, MG, and mango RNA aptamers following incubation of the triangular nanoparticles with their corresponding strands. Interestingly, the broccoli and MG RNA aptamers demonstrated high efficacy as molecular reporters with distinct magnitude of emission intensities. For example, the broccoli RNA aptamers were activated only in certain polygons such as square #2, pentagons #5 and #6, and hexagon #7. Similarly, the fluorescence from the MG-binding RNA aptamer was detected in square #1, pentagons #4 and #5, and hexagon #7. Additionally, the mango RNA aptamer showed higher fluorescence intensity in square #3, pentagons #4 and #5, as well as hexagon #7. However, due to the strong intrinsic background of TO1-biotin in solution and affinity to broccoli RNA aptamer,⁷² the mango aptamer reporting system exhibited a significant disadvantage compared to the MG and broccoli aptamers (Figure 4B, mango aptamer).

The samples numbered 1–7 were further analyzed under native conditions using 6% polyacrylamide gel electrophoresis to evaluate the formation of polygons. After electrophoresis was completed, the resulting gel was stained with a 5 μ M solution of DFHBI in TMS buffer and imaged using a Typhoon-5 Biomolecular Imaging system (Cytiva) with Cy2 channel ($\lambda_{\rm exc/em}$ = 488 nm/515–532 nm). The same gel was then stained with a 5 μ M solution of MG and subsequently imaged on a Typhoon-5 using a Cy5 channel ($\lambda_{\rm exc/em}$ = 635 nm/655–658 nm). Finally, an ethidium bromide (E.B.) solution was used to visualize the total RNA within the gel. The resulting images of the gel are shown in Figure 4C. The corresponding polygonal RNA complexes are clearly visible on the gels, with the exception of square #3 and pentagon #4 (both containing mango RNA aptamer that was originally designed to hybridize with rP6_Coli strand).

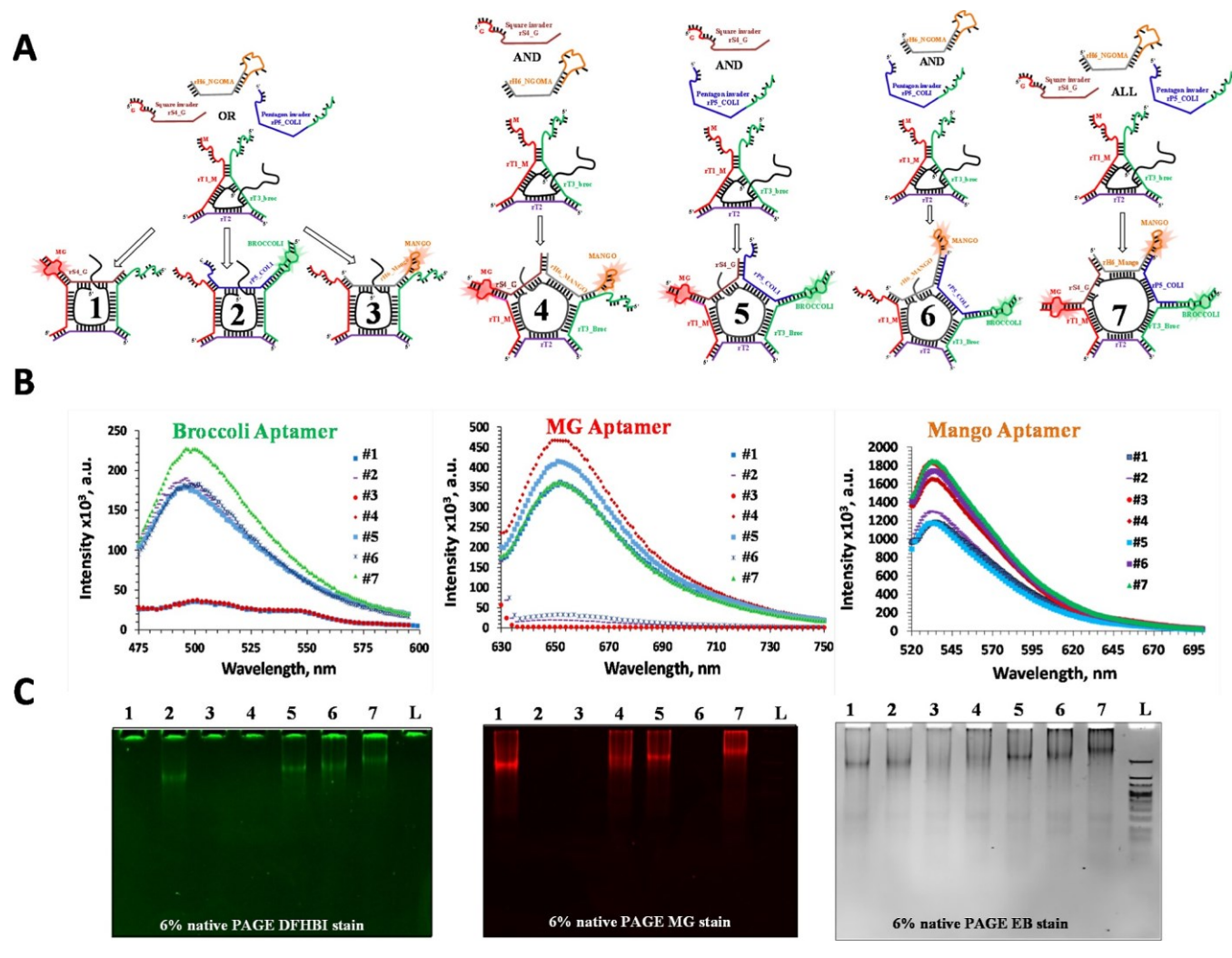


Figure 4. Analysis of non-sequential RNA shape reconfiguration. (A) Schematic diagram of possible 2D configurations of polygons. (B) Fluorescence properties of obtained polygons in solution. (C) Native PAGE analysis of each polygonal constructs. The gel was imaged after staining in DFHBI and MG solutions to detect signals from broccoli and MG RNA aptamers using Cy2 ($\lambda_{\rm exc/em}$ = 488 nm/515–532 nm) and Cy5 ($\lambda_{\rm exc/em}$ = 635 nm/655–658 nm) channels, respectively. To visualize total RNA, the gel was stained in a solution containing ethidium bromide. Lane L represents a low-molecular-weight DNA ladder from New England Biolabs.

Remarkably, the results obtained by non-sequential shape reconfigurations are suitable for the development of a threeinput AND logic gate. For example, the seven fluorogenic shapes described in this approach can be implied to perform the AND operation using a triangle nanoparticle with three binary ssRNA inputs: namely, rS4_G, rP5_Coli, and rH6_Ngoma, producing a binary output: a hexagonal nanoparticle with activation of all three light-up aptamers simultaneously, as shown in Table 2. Such a system, where three-input AND logic gate and three-output fluorogenic polygonal shapes, is an example of a complex circuit that can be served as a basis for further development of a biomolecular responsive nanodevice using the combination of specific ssRNA inputs. This feature makes the fluorogenic RNA nanoplatform a highly valuable tool in the field of synthetic biology.

Polygonal NANPs for the Cellular Uptake and Specific Gene Silencing. To explore the functional potential of the polygonal NANPs in vitro, cellular uptake and gene silencing assays were performed. In this critical set of experiments, the major aim was to demonstrate that

Table 2. Three-Input AND Logic Gate Truth Table

ssRNA INPUTS		OUTPUT			
rS4_G	rP5_Coli	rH6_Mango	SQR	PENT	HEX
1	0	0	1	0	0
0	1	0	1	0	0
0	0	1	1	0	0
1	1	0	0	1 1	0
1	0	1	0	1 1	0
0	1	1	0	1 1	0
1	1	1	0	0	1 1 1

reconfigurable fluorogenic reporters can be eventually implemented within the intracellular environment for bioanalysis, sensing, and imaging of therapeutic and diagnostic nanoparticles. In our previous reports, 12,31,61,62 we thoroughly studied the physicochemical properties of polygonal complexes made of RNA, DNA, and their hybrids assemblies. As shown in Figure 5, only the RNA polygons stimulate significant production of the pro-inflammatory cytokine, IL-6, and the

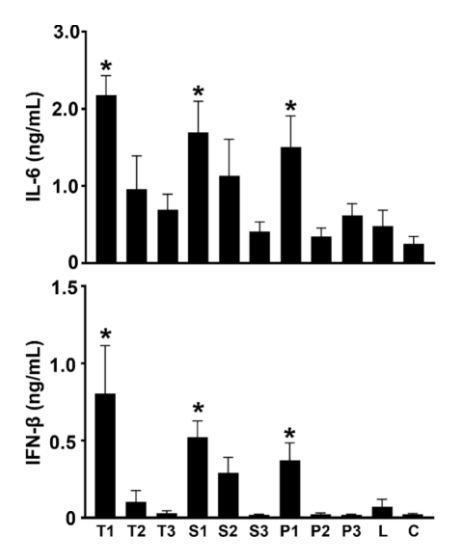


Figure 5. Assessment of nucleic acid nanoparticle immunostimulation. NANPs composed of only RNA stimulate significant production of IL-6 and IFN- β . The cell line, h μ glia, was transfected with NANPs at the final concentration of 5 nM. NANPs T1-3 are triangles composed of RNA, a DNA center with outer RNA strands, or DNA, respectively. NANPs S1-3 are squares composed of RNA, a DNA center with outer RNA strands, or DNA, respectively. NANPs P1-3 are pentagons composed of RNA, a DNA center with outer RNA strands, or DNA, respectively. L indicated the lipofectamine 2000 control, and C indicated untreated cells. Cell supernatants were collected 24 h post transfection. IL-6 and IFN- β production was quantified using specific capture ELISAs. Data are expressed as the mean \pm SEM for a minimum of three independent replicates. Asterisks indicated statistical significance compared to untreated cells. (C) Student's *t*-test, *p* < 0.05.

type 1 interferon, IFN- β . In contrast, hybrid polygons displayed reduced IL-6 and IFN- β production compared to RNA polygon- and DNA polygon-stimulated minimal responses. Additionally, neither the RNA nor the DNA duplex stimulated IL-6 or IFN- β production. Collectively, this indicates that incorporation of DNA strands provides an approach to reduce the stimulation of cellular cytokine and interferon responses. Therefore, these polygon scaffolds can be optimized to avoid unwanted or achieve desired immune stimulation. Justified by the results that hybrid RNA/DNA-center NANPs demonstrated optimal profiles for thermal and enzymatic stability in blood serum as well as exhibited insignificant levels of immune response, the hybrid polygons

were utilized in all in vitro assays. The secondary structure and sequences for the hybrid polygons are available in Supporting Information Figure S10. The assembly of the individual polygons with various numbers of functional single-stranded oligonucleotides was confirmed by the means of gel electrophoresis, as shown in Figure 6. Noteworthy, the regioselective positions of the functional oligonucleotides can be precisely controlled by variation of sticky-ends and blunt-ends RNA according to previously reported findings utilizing triangle NPs only.61 Assembled hybrid NPs were decorated with either fluorescently labeled ssDNA-Alexa 546 for cellular uptake studies or with siRNA targeting green fluorescent protein (GFP) for specific gene silencing. All in vitro assays were conducted using human breast cancer cells (MDA-MB-231). In the internalization studies, a lipofectamine-transfecting reagent was used to facilitate the intracellular uptake of fluorescently labeled polygons with subsequent analysis by fluorescent microscopy Figure 7A. The results demonstrate effective transfection efficiencies for nanoparticles that are comparable to the uptake of free fluorescently labeled DS DNAs tested at the same 10 nM final concentration of DS

The successful dicer-assisted intracellular release of siRNAs and activation of RNA interference were further tested on GFP expressing breast cancer cells. The cells were transfected with polygonal constructs functionalized with maximum anti-GFP siRNA payloads and compared to free anti-GFP DS RNAs (Figure 7B,C). The results demonstrate GFP silencing of greater than 90% with comparable efficiencies among polygons and DS RNA at nanomolar concentrations. The combination of the cellular uptake and specific gel silencing assays clearly indicate that the nucleic acid polygons can be used as a dynamic scaffold for delivery of siRNAs and fluorescent probes to the diseased human cells.

CONCLUSIONS

We have described an innovative design approach to fabricate dynamic NANPs by combining toehold-mediated strand displacement and split fluorogenic RNA aptamer techniques. We first have experimentally validated effective non-reversible, sequential shape switching from a DNA triangle to a square to a pentagon and to a hexagon containing 10 nt. toehold regions. The transition principle is based on using central fuel and invader DNA strands encompassing sequences that correspond to the individual DNA polygons. This strategy was further implemented to fabricate responsive RNA polygonal NANPs

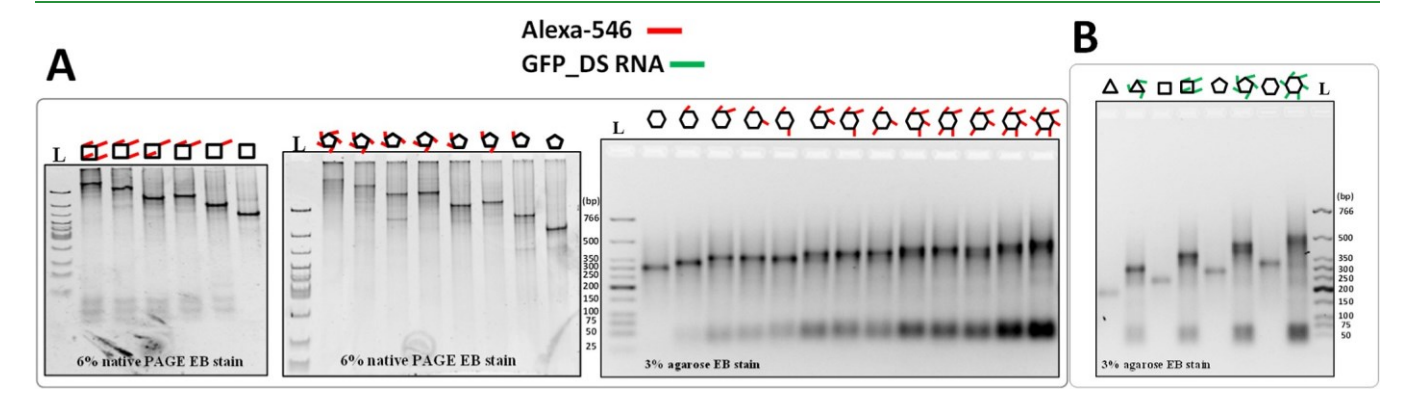


Figure 6. Electrophoretic mobility shift assays of polygonal NANPs harboring Alexa-488 labeled ODN (A) and GFP-targeting antisense RNA (B). Lane L corresponds to the DNA ladder (low-molecular weight, New England Biolabs).

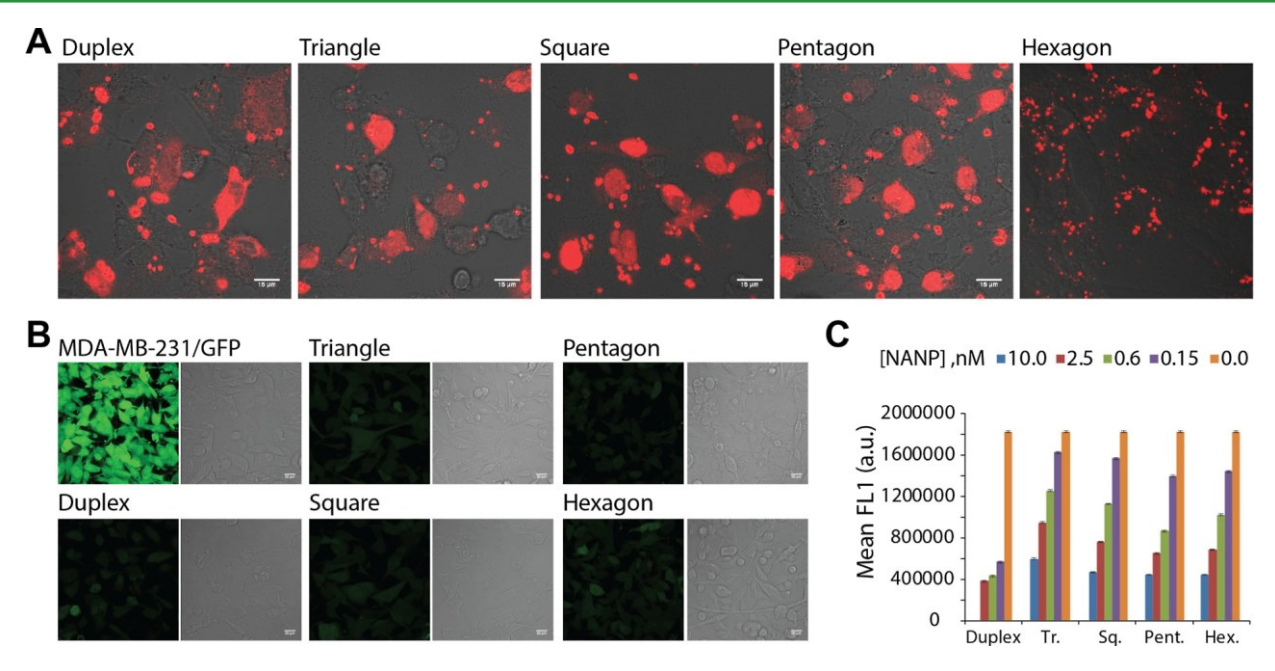


Figure 7. Cellular uptake and gene-specific silencing assays. The experiments performed using human breast cancer cell line (MDA-MB-231) with and without GFP. (A) Fluorescent microscopy of non-fluorescent cells 24 h post-transfection with Alexa 546-labeled polygons and DS RNAs (10 nM final DS RNA) is shown. (B) Analysis of GFP-expressing cells 4 days post-transfection with anti-GFP DS RNA-functionalized polygons and DS RNA (10 nM final DS RNA) by a fluorescent microscope and subsequent fluorescence quantification by flow cytometry. (C) Error bars indicate \pm SEM.

ı

emitting distinct fluorescence. The effective shape switching can be monitored in solution by measuring fluorescence emission of three RNA aptamers, MG, broccoli, and mango. Based on the corresponding fluorescence emissions, one can predict the presence of a particular nanoparticle shape from a given set of solutions. A non-fluorescent sample indicates the presence of triangular particles only. The emission from the MG aptamer corresponds to the presence of either square, pentagon, or hexagon NANPs. Fluorescent signals from MG and broccoli aptamers suggest the presence of pentagonal nanoconstruct. The presence of hexagonal RNA nanoparticle can be determined only if all corresponding RNA aptamers exhibit distinct emissions.

We also demonstrated that RNA fluorogenic aptamer systems can incorporate AND logic gates into fluorophore-based detection systems. Multiple fluorophores with different excitation and emission spectra (such as MG, broccoli, and mango) can be used, and each can be linked to a different input molecule. For instance, in a three-input AND gate system, a detection assay can be designed where the presence of all three ssRNA input molecules activates all three fluorophores, resulting not only in a specific fluorescence pattern but also in specific polygonal shape configuration that indicates the presence of all three inputs. This approach can lead to the development of highly specific and sensitive detectors for particular combinations of inputs, making them useful for various applications such as biosensing and diagnostic assays.

To further validate feasibility of the design of functional dynamic polygonal nanodevice in vitro, we have conducted a series of experiments using human breast cancer cells. In particular, we studied the cellular uptake and specific gene silencing for polygons. We used a hybrid RNA/DNA-center polygonal platform for the following reasons: (i) such hybrids are stable in blood serum and (ii) non-immunogenic enabling

the transition from in vitro assays to further implementation in mouse models. Our results showed efficient cellular uptake and effective GFP silencing by all polygonal NANPs, demonstrating feasibility of this nanoplatform for further development of smart nanodevices. Additionally, our data further support that polygon nucleic acid composition can be optimized to avoid or enhance cell innate immune responses. Importantly, we have observed that hybrid polygons possess optimal thermal and enzymatic stability and stimulate minimal proinflammatory and interferon responses. Although this project is still in its development stage, our data serve as an important validation of the applicability and feasibility of dynamic nucleic acid polygon systems to construct "smart" nanodevices based on shape transition. Furthermore, we anticipate designing and further applying dynamic, polygonal NANPs that would carry split or misfolded functional nucleic acids (e.g., Dicer substrate RNAs) which could be activated intracellularly upon binding to specific target sequences indicative of a diseased state, through refolding or reassembly processes.³⁰ This research and future work may have implications for synthetic biology, drug delivery, and gene silencing fields. For example, the nucleic acid nanodevices have the potential to become responsive nanovehicles with a built-in programmable release of its cargo upon sensing oncogenic RNA.

MATERIALS AND METHODS

Nucleic Acid Sequence Design, Synthesis, and Assembly. The core DNA and cognate RNA polygonal sequences containing tetra U/T-motifs were obtained from previously published reports. 12,61 The design of ssDNA toehold region on the triangle and corresponding invader oligonucleotides was carried out using the multi-strand secondary structure prediction programs NUPACK and *mfold*. 64,73 The sequence selection criterion was based on the calculated lowest free-energy secondary structure of the desired DNA or RNA polygons. The sequence selection was made to ensure

that no other unwanted formation of secondary structures was closer than 15% in energy to the lowest energy structure.

The sequences of GFP_DS RNA and DNA oligonucleotides including long DNA fuel strand were purchased from IDT DNA (www.idtdna.com) as desalted products and used without purification. The cognate RNA strands with corresponding RNA aptamer regions were synthesized by run-off transcription of PCR-amplified DNA templates using "home-made" T7 RNA polymerase with the TAATACGACTCACTATA promoter region⁶¹ (Supporting Information Figure S5). PCR products were purified using the QiaQuick PCR purification kit (Qiagen Sciences, Maryland 20874) prior in the vitro transcription reaction. All transcribed RNA products were purified by denaturing 20% polyacrylamide gel (29:1 acrylamide/bisacrylamide) electrophoresis (PAGE) containing 8 M UREA.¹⁵

The co-transcriptional synthesis of the RNA hexagonal complex was achieved by introducing seven corresponding purified PCR DNA templates into an in vitro T7 RNA transcription mixture, with equal ratios. After 4 hours of incubation at 37 °C, DNase I treatment was applied to remove the DNA sequences, and the resulting crude RNA product was analyzed using gel shift assay and fluorescence study without purification.

Individual DNA and RNA polygon self-assembly was achieved by mixing corresponding equimolar oligonucleotide strands (1 μ M) in TMS buffer (50 mM TRIS pH = 8.0, 100 mM NaCl, and 10 mM MgCl₂), heating the mixture to +80 °C, and gradually cooling it to +4 °C over a period of 1 h on a PCR thermocycler. The assembly efficiencies were determined by native PAGE. An equal amount of gel loading buffer [sucrose 40% (wt/vol), 0.1% (wt/vol) xylene cyanol, and 0.1% (wt/vol) bromophenol blue] was added to each sample. Samples were run at ambient temperature on 6% native polyacrylamide gels (29:1 acrylamide/bisacrylamide) in TBM buffer (tris base 89 mM, boric acid 200 mM, and MgCl₂ 5 mM T) at constant 80 V. The gels were subsequently stained with either 5 μ M MG solution in 1× TMS, 5 μ M DFHBI in 1× TMS solution, or concentrated ethidium bromide solution, and imaged using either a GhemiDoc XRS (BioRad) or Typhoon-5 (Cytiva) imaging system.

The nucleic acid complexes can also be resolved by agarose gel electrophoresis containing E.B. in $1 \times TAE$ buffer.

Toehold-Mediated Nucleic Acid Shape Transition Experiments. To the annealed DNA or RNA triangle nanoparticles, typically 1 µM in TMS buffer, a small amount of corresponding square invader DNA or RNA molecules were added to achieve 1:1 stoichiometric ratio. The mixture was then incubated in a water bath at 37 °C for 30 min or on the bench at room temperature (RT), allowing strand displacement reaction to reach equilibrium. After obtaining an aliquot for subsequent analysis by gel electrophoresis, the small amount of pentagon DNA invader was added to the same sample vial to achieve 1:1 stoichiometry. Following the incubation step, an aliquot was taken for gel analysis. The above procedure was repeated using final hexagon invading strand. Importantly, to prevent any possible annealing that could occur as a result of slow cooling from 37 °C to RT, the aliquots were immediately mixed with a sample loading buffer that was kept on ice and stored at -20 °C prior to analysis. The corresponding aliquots were subjected to 6% native PAGE or 4% agarose gel electrophoretic analysis to confirm the shape

The calculation of the yield (%) of successful transformation from triangular to square to pentagonal and hexagonal nanoparticles was conducted by analyzing electrophoretic gel images using ImageJ software. ⁶⁷ The band densities corresponding to individual polygons after transformation were compared to the corresponding annealed complexes obtained by "one-pot" assembly.

The non-sequential shape reconfiguration using toehold-mediated strand displacement approach was conducted in the same manner as described above. The annealed triangular nanoparticles (1 μ M in 1× TMS) were mixed with an equimolar amount of either an individual invading strand, two invaders, or all three invaders. The solution was incubated at 37 °C for 30 min, and the resulting product was immediately placed on ice and mixed with gel loading buffer for subsequent analysis on PAGE.

Fluorescence Measurements. The fluorescence experiments in solution were performed using a FluoroMax 3 (Jobin Yvon) fluorescence spectrometer, unless specified otherwise. A sub-micro quartz fluorometer cell from Starna cells, Inc. was used for the experiments. RNA samples (100 μ L) were assembled at 0.5 μ M concentrations of individual strands in TMS buffer. A concentrated solutions of each fluorophores MG (N,N,N',N'-tetramethyl-4,4'diaminotriphenylcarbenium chloride, Sigma-Aldrich), DFHBI [(5Z)-5-[(3,5-difluoro-4-hydroxyphenyl)methylene]-3,5-dihydro-2,3-dimethyl-4*H*-imidazole-4-one, (Z)-4-(3,5-difluoro-4-hydroxybenzylidene)-1,2-dimethyl-1H-imidazole-5(4H)-one, Sigma-Aldrich], and TO1-3PEG-biotin (Applied Biological Materials Inc, Abmgood) was added to assembled RNA complexes to reach 5 µM final concentration of each dye. The mixture was allowed to equilibrate at RT for at least 15 min to facilitate binding of the fluorophores to corresponding RNA aptamers. For the MG-binding RNA aptamer, the excitation wavelength centered at 615 nm, and emission was collected in the range of 630-700 nm; for the broccoli RNA aptamer, the excitation was centered at 465 nm, and emission was recorded from the range of 475–650 nm; for the TO1-bioting-binding mango aptamer, the fluorescence spectra were collected from 520 to 650 nm with the excitation wavelength of 510 nm.

Dynamic Light Scattering Analysis. The average dimensions of the assembled RNA polygons were measured at concentrations of 1 μ M in 100 μ L of TMS buffer using Zetasizer nano-ZS (Malvern Instrument, LTD) at 25 °C according to previously described protocol. ¹² The hydrodynamic diameters were calculated by fitting data points to a Gaussian distribution.

Atomic Force Microscopy Imaging. The samples of each RNA and DNA polygons were purified using gel electrophoresis prior to imaging. The assembled DNA and RNA polygons (2 μ M concentration of each strand, in 50 μ L TMS buffer) were subjected to the 6% native PAGE. After band visualization by UV-shadowing, the gel pieces with corresponding nucleic acid complexes were cut and eluted overnight into 200 μ L of TMS buffer. The samples were concentrated using a 3KDa molecular-weight cutoff filter device (Ultracel-3, Millipore) and resuspended into 100 μ L of TMS buffer. AFM imaging was conducted at RT using silicon probes (NCH 320 kHz resonance frequency and 42 N/m spring constant, www.nanoworld.com) on the MultiMode AFM NanoScope IV system (Veeco), following the well-developed protocol.⁷⁴

Specific Gene Silencing Experiments. *Transfection Experiments.* To assess the delivery and intracellular activity of functionalized hybrid nanoparticles, the human breast cancer cell line *MDA-MB-231* (with or without GFP) was grown in D-MEM medium (Gibco BRL) supplemented with 10% FBS and penicillinstreptomycin (pen-strep) in a 5% CO₂ incubator. Lipofectamine 2000 (L2K, Invitrogen) was used in all transfection experiments. Transfection solutions (100×) were pre-incubated at RT with L2K. The cell media was replaced with OPTI-MEM with added RNA/L2K complexes at a final concentration of 1× prior to each transfection. The cells were incubated for 4 h followed by the media replacement (D-MEM, 10% FCS, 1% pen-strep).

Microscopy. The silencing experiments were visualized using a UV 510 confocal microscope (Carl Zeiss, Oberkochen) and a Plan-Neofluar 40×/1.3 oil lens. MDA-MB-231 eGFP cells were plated in glass bottom dishes (Ibidi, Madison), transfected as described above. 3 days upon transfection, the cells were washed three times with PBS and fixed with 4% paraformaldehyde for 20 min at RT for imaging. For GFP imaging, the 488 nm line of an argon laser was used as excitation, and emission was collected using a BP 505-550 filter. The uptake experiments were visualized using a LSM 710 confocal microscope (Carl Zeiss, Oberkochen) and a Plan-Apochromat 63×/ 1.40 oil lens. MDA-MB-231 cells were transfected with Alexa 456 fluorescently labeled nanoconstructs. The next day, cells were washed three times with PBS and fixed with 4% paraformaldehyde for 20 min at RT for imaging. For Alexa 546 imaging, a DPSS 561 laser was used for excitation, and emission was collected between 566 and 680 nm. Flow Cytometry. For flow cytometry experiments, MDA-MB-231 cells (with or without GFP) plated in 24-well plates were transfected.

The cells were analyzed 24 h later to assess their level of Alexa 546 fluorescence or 72 h later to assess their GFP signal for uptake and silencing experiments, respectively. The measurements were performed through fluorescence-activated cell sorting on a FACScalibur instrument (BD Biosciences, San Jose) or on a Acurri C6 instrument (BD Biosciences, San Jose). At least 20,000 events were collected and analyzed with CellQuest or CFlow Sampler software to retrieve the geometric mean fluorescence intensity and the standard error of the mean.

Assessment of Nucleic Acid Nanoparticle Immunostimula**tory Properties.** The cell line, $h\mu$ glia, was provided by Dr. Jonathan Karn (Case Western Reserve University) and maintained in Dulbecco's modified Eagle's medium supplemented with 5% FBS and penicillin/streptomycin (100 U/mL to 100 µg/mL). According the manufacturer's guidelines, cells were transfected with NANPs (5 nM) for 4 h using lipofectamine 2000. Cell supernatants were collected at 24 h post transfection. Human IL-6 and IFN-β production was quantified via specific capture ELISAs. IL-6 capture ELISAs were conducted using a rat anti-human IL-6 capture antibody (BD Pharmingen, cat# 554543, Clone Mq2-13A5) and a biotinylated rat anti-human IL-6 detection antibody (BD Pharmingen, cat# 554546, Clone MQ2-39C3). IFN- β capture ELISAs were conducted using a polyclonal rabbit anti-human IFN-β capture antibody (Abcam, cat# ab186669) and a biotinylated polyclonal rabbit anti-human IFN- β detection antibody (Abcam, cat# ab84258). Streptavidin-horseradish peroxidase (BD Biosciences) was added prior to the tetramethylbenzidine substrate to detect bound antibody. H₂SO₄ was used to stop the reaction, and the absorbance was measured at 450 nm. A standard curve was generated using recombinant IL-6 (BD Pharmingen) and IFN- β (Abcam). The concentration of cytokines in cell supernatants was then determined by extrapolation of the absorbance to the standard curve.

_

ASSOCIATED CONTENT

Supporting Information

The Supporting Information is available free of charge at https://pubs.acs.org/doi/10.1021/acsami.3c01604.

Oligonucleotide sequences used in this project; sequences and 2D structures of the DNA polygons and fluorogenic RNA polygons; design principle of mango RNA aptamer reporter; comparison of specific DNA shape transformations and sequential RNA shape transformations at ambient and physiological temperatures; fluorescence analysis of the co-transcriptional product of the hexagonal NANP; fluorescence intensity changes in the presence of ssRNA inputs; DNA polygon assembly properties from various strands evaluated by agarose gel electrophoresis; RNA polygon assembly properties evaluated by agarose gel electrophoresis; sequences and 2D structures of the RNA–DNA hybrid polygons used for in vitro assays; and agarose gel electrophoresis analysis (PDF)

AUTHOR INFORMATION

Corresponding Authors

Kirill A. Afonin — Department of Chemistry, University of North Carolina at Charlotte, Charlotte, North Carolina 28223, United States; orcid.org/0000-0002-6917-3183; Email: kafonin@uncc.edu

Emil F. Khisamutdinov — Department of Chemistry, Ball State University, Muncie, Indiana 47306, United States;
orcid.org/0000-0002-1568-4412; Email: kemil@bsu.edu

Authors

Jordan Hartung — Department of Chemistry, Ball State University, Muncie, Indiana 47306, United States Nathan McCann — Department of Chemistry, Ball State
University, Muncie, Indiana 47306, United States
Erwin Doe — Department of Chemistry, Ball State University,
Muncie, Indiana 47306, United States
Hannah Hayth — Department of Chemistry, Ball State
University, Muncie, Indiana 47306, United States
Kheiria Benkato — Department of Chemistry, Ball State
University, Muncie, Indiana 47306, United States
M. Brittany Johnson — Department of Biology, University of
North Carolina at Charlotte, Charlotte, North Carolina

Mathias Viard — Laboratory of Integrative Cancer Immunology, Center for Cancer Research, National Cancer Institute, Bethesda, Maryland 20892, United States; Basic Science Program, Leidos Biomedical Research Inc. National Cancer Institute, National Institutes of Health, Frederick, Maryland 21702, United States

Complete contact information is available at: https://pubs.acs.org/10.1021/acsami.3c01604

Author Contributions

28223, United States

J.H., N.M., and E.D. contributed equally to this work. E.F.K. and K.A.A. devised the project, provided the main conceptual ideas, and designed the experimental study. J.H. and E.D. performed fluorescence experiments. J.H., N.M., K.B., and H.H. carried out assembly, RNA synthesis, and purification experiments. M.V. performed in vitro uptake and gene silencing cell studies. M.B.J. carried out immunological studies. E.F.K. and K.A.A. co-wrote the manuscript. All authors provided critical feedback to the manuscript. All authors have given approval to the final version of the manuscript.

Notes

The authors declare no competing financial interest.

ACKNOWLEDGMENTS

Authors are thankful to Dr. Alexander Lushnikov and Dr. Alexey Krasnoslobodtsev for performing AFM imaging of the polygonal nanoparticles at the nanoimaging core facility at the University of Nebraska Medical Center. This work was supported by NIH grant 1R15EB031388-01 and NSF MRI award number 2214573 to E.F.K. Also, research reported in this publication was supported in part by the National Institute of General Medical Sciences of the National Institutes of Health under award number R35GM139587 (to K.A.A.). The content is solely the responsibility of the authors and does not necessarily represent the official views of the National Institutes of Health. This project has been funded in whole or in part with federal funds from the Frederick National Laboratory for Cancer Research under contract no. HHSN261200800001E. The content of this publication neither necessarily reflects the views or policies of the Department of Health and Human Services nor does mention trade names, commercial products, or organizations imply endorsement by the US Government. Research reported in this publication was in part supported by the National Science Foundation, Division of Material Research: Award Numbers DMR-2203946 (to K.A.A.)

REF

REFERENCES

(1) Krishna, R. H.; Chandraprabha, M. N.; Monika, P.; Br, T.; Chaudhary, V.; Manjunatha, C. Biomolecule conjugated inorganic

- nanoparticles for biomedical applications: A review. *Biotechnol. Genet. Eng. Rev.* 2022, 1–42.
- (2) Varshosaz, J.; Taymouri, S. Hollow Inorganic Nanoparticles as Efficient Carriers for siRNA Delivery: A Comprehensive Review. *Curr. Pharm. Des.* 2015, *21*, 4310–4328.
- (3) Cruz-Acuna, M.; Halman, J. R.; Afonin, K. A.; Dobson, J.; Rinaldi, C. Magnetic nanoparticles loaded with functional RNA nanoparticles. *Nanoscale* 2018, *10*, 17761–17770.
- (4) Perumal, S.; Atchudan, R.; Lee, W. A Review of Polymeric Micelles and Their Applications. *Polymers* 2022, *14*, 2510.
- (5) Chiu, M. L.; Goulet, D. R.; Teplyakov, A.; Gilliland, G. L. Antibody Structure and Function: The Basis for Engineering Therapeutics. *Antibodies* 2019, 8, 55.
- (6) Fernandez, L. A.; Muyldermans, S. Recent developments in engineering and delivery of protein and antibody therapeutics. *Curr. Opin. Biotechnol.* 2011, 22, 839–842.
- (7) Vishweshwaraiah, Y. L.; Hnath, B.; Rackley, B.; Wang, J.; Gontu, A.; Chandler, M.; Afonin, K. A.; Kuchipudi, S. V.; Christensen, N.; Yennawar, N. H.; Dokholyan, N. V. Adaptation-proof SARS-CoV-2 vaccine design. *Adv. Funct. Mater.* 2022, *32*, 2206055.
- (8) Michelotti, N.; Johnson-Buck, A.; Manzo, A. J.; Walter, N. G. Beyond DNA origami: the unfolding prospects of nucleic acid nanotechnology. *Wiley Interdiscip. Rev.: Nanomed. Nanobiotechnol.* 2012, 4, 139–152.
- (9) Guo, P. The emerging field of RNA nanotechnology. *Nat. Nanotechnol.* 2010, *5*, 833–842.
- (10) Afonin, K. A.; Dobrovolskaia, M. A.; Ke, W.; Grodzinski, P.; Bathe, M. Critical review of nucleic acid nanotechnology to identify gaps and inform a strategy for accelerated clinical translation. *Adv. Drug Deliv. Rev.* 2022, *181*, 114081.
- (11) Durbin, J. K.; Miller, D. K.; Niekamp, J.; Khisamutdinov, E. F. Modulating Immune Response with Nucleic Acid Nanoparticles. *Molecules* 2019, *24*, 3740.
- (12) Johnson, M. B.; Halman, J. R.; Satterwhite, E.; Zakharov, A. V.; Bui, M. N.; Benkato, K.; Goldsworthy, V.; Kim, T.; Hong, E.; Dobrovolskaia, M. A.; Khisamutdinov, E. F.; Marriott, I.; Afonin, K. A. Programmable Nucleic Acid Based Polygons with Controlled Neuroimmunomodulatory Properties for Predictive QSAR Modeling. *Small* 2017, 13, 1701255.
- (13) Leontis, N. B.; Stombaugh, J.; Westhof, E. The non-Watson-Crick base pairs and their associated isostericity matrices. *Nucleic Acids Res.* 2002, *30*, 3497–3531.
- (14) Leontis, N. B.; Westhof, E. Geometric nomenclature and classification of RNA base pairs. *RNA* 2001, 7, 499–512.
- (15) Khisamutdinov, E. F.; Sweeney, B. A.; Leontis, N. B. Context-sensitivity of isosteric substitutions of non-Watson-Crick basepairs in recurrent RNA 3D motifs. *Nucleic Acids Res.* 2021, *49*, 9574–9593.
- (16) Leontis, N. B.; Lescoute, A.; Westhof, E. The building blocks and motifs of RNA architecture. *Curr. Opin. Struct. Biol.* 2006, *16*, 279–287.
- (17) Leontis, N. B.; Westhof, E. The annotation of RNA motifs. *Comp. Funct. Genomics* 2002, *3*, 518–524.
- (18) Khisamutdinov, E. F.; Jasinski, D. L.; Guo, P. RNA as a boiling-resistant anionic polymer material to build robust structures with defined shape and stoichiometry. *ACS Nano* 2014, *8*, 4771–4781.
- (19) Jaeger, L.; Leontis, N. B. Tecto-RNA: One-Dimensional Self-Assembly through Tertiary Interactions. *Angew Chem., Int. Ed.* 2000, 39, 2521–2524.
- (20) Novikova, I. V.; Hassan, B. H.; Mirzoyan, M. G.; Leontis, N. B. Engineering cooperative tecto-RNA complexes having programmable stoichiometries. *Nucleic Acids Res.* 2011, *39*, 2903–2917.
- (21) Afonin, K. A.; Lin, Y. P.; Calkins, E. R.; Jaeger, L. Attenuation of loop-receptor interactions with pseudoknot formation. *Nucleic Acids Res.* 2012, *40*, 2168–2180.
- (22) Parsons, M. F.; Allan, M. F.; Li, S.; Shepherd, T. R.; Ratanalert, S.; Zhang, K.; Pullen, K. M.; Chiu, W.; Rouskin, S.; Bathe, M. 3D RNA-scaffolded wireframe origami. *Nat. Commun.* 2023, 14, 382.

- (23) Veneziano, R.; Ratanalert, S.; Zhang, K.; Zhang, F.; Yan, H.; Chiu, W.; Bathe, M. Designer nanoscale DNA assemblies programmed from the top down. *Science* 2016, *352*, 1534.
- (24) Wang, X.; Li, S.; Jun, H.; John, T.; Zhang, K.; Fowler, H.; Doye, J. P. K.; Chiu, W.; Bathe, M. Planar 2D wireframe DNA origami. *Sci. Adv.* 2022, *8*, No. eabn0039.
- (25) Chandler, M.; Afonin, K. A. Smart-Responsive Nucleic Acid Nanoparticles (NANPs) with the Potential to Modulate Immune Behavior. *Nanomaterials* 2019, *9*, 611.
- (26) Halman, J. R.; Satterwhite, E.; Roark, B.; Chandler, M.; Viard, M.; Ivanina, A.; Bindewald, E.; Kasprzak, W. K.; Panigaj, M.; Bui, M. N.; Lu, J. S.; Miller, J.; Khisamutdinov, E. F.; Shapiro, B. A.; Dobrovolskaia, M. A.; Afonin, K. A. Functionally-interdependent shape-switching nanoparticles with controllable properties. *Nucleic Acids Res.* 2017, *45*, 2210–2220.
- (27) Bindewald, E.; Afonin, K. A.; Viard, M.; Zakrevsky, P.; Kim, T.; Shapiro, B. A. Multistrand Structure Prediction of Nucleic Acid Assemblies and Design of RNA Switches. *Nano Lett.* 2016, *16*, 1726–1735
- (28) Chandler, M.; Lyalina, T.; Halman, J.; Rackley, L.; Lee, L.; Dang, D.; Ke, W.; Sajja, S.; Woods, S.; Acharya, S.; Baumgarten, E.; Christopher, J.; Elshalia, E.; Hrebien, G.; Kublank, K.; Saleh, S.; Stallings, B.; Tafere, M.; Striplin, C.; Afonin, K. A. Broccoli Fluorets: Split Aptamers as a User-Friendly Fluorescent Toolkit for Dynamic RNA Nanotechnology. *Molecules* 2018, *23*, 3178.
- (29) Afonin, K. A.; Lindsay, B.; Shapiro, B. A. Engineered RNA Nanodesigns for Applications in RNA Nanotechnology. *DNA RNA Nanotechnol.* 2013, *1*, 1–15.
- (30) Zakrevsky, P.; Parlea, L.; Viard, M.; Bindewald, E.; Afonin, K. A.; Shapiro, B. A. Preparation of a Conditional RNA Switch. *Methods Mol. Biol.* 2017, *1632*, 303–324.
- (31) Ke, W.; Hong, E.; Saito, R. F.; Rangel, M. C.; Wang, J.; Viard, M.; Richardson, M.; Khisamutdinov, E. F.; Panigaj, M.; Dokholyan, N. V.; Chammas, R.; Dobrovolskaia, M. A.; Afonin, K. A. RNA–DNA fibers and polygons with controlled immunorecognition activate RNAi, FRET and transcriptional regulation of NF-κB in human cells. *Nucleic Acids Res.* 2019, *47*, 1350–1361.
- (32) Yourston, L.; Rolband, L.; West, C.; Lushnikov, A.; Afonin, K. A.; Krasnoslobodtsev, A. V. Tuning properties of silver nanoclusters with RNA nanoring assemblies. *Nanoscale* 2020, *12*, 16189–16200.
- (33) Sinitsyna, V. V.; Vetcher, A. A. Nucleic Acid Aptamers in Nanotechnology. *Biomedicines* 2022, 10, 1079.
- (34) Panigaj, M.; Johnson, M. B.; Ke, W.; McMillan, J.; Goncharova, E. A.; Chandler, M.; Afonin, K. A. Aptamers as Modular Components of Therapeutic Nucleic Acid Nanotechnology. *ACS Nano* 2019, *13*, 12301–12321.
- (35) Zhang, D. Y.; Seelig, G. Dynamic DNA nanotechnology using strand-displacement reactions. *Nat. Chem.* 2011, *3*, 103–113.
- (36) Yang, Y.; Wang, W.; Liu, H.; Tong, L.; Mu, X.; Chen, Z.; Tang, B. Sensitive Quantification of MicroRNA in Blood through Multiamplification Toehold-Mediated DNA-Strand-Displacement Paper-Spray Mass Spectrometry (TSD-PS MS). *Angew Chem.*, *Int. Ed.* 2022, *61*, No. e202113051.
- (37) Zakrevsky, P.; Bindewald, E.; Humbertson, H.; Viard, M.; Dorjsuren, N.; Shapiro, B. A. A Suite of Therapeutically-Inspired Nucleic Acid Logic Systems for Conditional Generation of Single-Stranded and Double-Stranded Oligonucleotides. *Nanomaterials* 2019, *9*, 615.
- (38) Yurke, B.; Mills, A. P., Jr.; Lai Cheng, S. DNA implementation of addition in which the input strands are separate from the operator strands. *Biosystems* 1999, *52*, 165–174.
- (39) Yurke, B.; Turberfield, A. J.; Mills, A. P., Jr.; Simmel, F. C.; Neumann, J. L. A DNA-fuelled molecular machine made of DNA. *Nature* 2000, 406, 605–608.
- (40) Hu, H.; Zhou, F.; Wang, B.; Chang, X.; Dai, T.; Tian, R.; Wan, Y.; Wang, X.; Wang, G. Autonomous operation of 3D DNA walkers in living cells for microRNA imaging. *Nanoscale* 2021, *13*, 1863–1868.

- (41) Nummelin, S.; Shen, B.; Piskunen, P.; Liu, Q.; Kostiainen, M. A.; Linko, V. Robotic DNA Nanostructures. *ACS Synth. Biol.* 2020, *9*, 1923–1940.
- (42) Gianneschi, N. C.; Ghadiri, M. R. Design of molecular logic devices based on a programmable DNA-regulated semisynthetic enzyme. *Angew Chem. Int. Ed.* 2007, *46*, 3955–3958.
- (43) Liu, S.; Jiang, Q.; Wang, Y.; Ding, B. Biomedical Applications of DNA-Based Molecular Devices. *Adv. Healthcare Mater.* 2019, 8, No. e1801658.
- (44) Kuzuya, A.; Ohya, Y. Nanomechanical molecular devices made of DNA origami. *Acc. Chem. Res.* 2014, 47, 1742–1749.
- (45) Acevedo-Rocha, C. G.; Reetz, M. T. Assembly of Designed Oligonucleotides: a useful tool in synthetic biology for creating high-quality combinatorial DNA libraries. *Methods Mol. Biol.* 2014, *1179*, 189–206.
- (46) Vecchioni, S.; Capece, M. C.; Toomey, E.; Nguyen, L.; Ray, A.; Greenberg, A.; Fujishima, K.; Urbina, J.; Paulino-Lima, I. G.; Pinheiro, V.; Shih, J.; Wessel, G.; Wind, S. J.; Rothschild, L. Construction and characterization of metal ion-containing DNA nanowires for synthetic biology and nanotechnology. *Sci. Rep.* 2019, *9*, 6942.
- (47) Goldsworthy, V.; LaForce, G.; Abels, S.; Khisamutdinov, E. F. Fluorogenic RNA Aptamers: A Nano-platform for Fabrication of Simple and Combinatorial Logic Gates. *Nanomaterials* 2018, 8, 984.
- (48) Bouhedda, F.; Autour, A.; Ryckelynck, M. Light-Up RNA Aptamers and Their Cognate Fluorogens: From Their Development to Their Applications. *Int. J. Mol. Sci.* 2017, *19*, 44.
- (49) Ouellet, J. RNA Fluorescence with Light-Up Aptamers. Front. Chem. 2016, 4, 29.
- (50) Endoh, T.; Mie, M.; Kobatake, E. Direct detection of RNA transcription by FRET imaging using fluorescent protein probe. *J. Biotechnol.* 2008, *133*, 413–417.
- (51) Wadsworth, G. M.; Parikh, R. Y.; Kim, H. D. Dual-probe RNA FRET-FISH in Yeast. *Bio-Protoc.* 2018, 8, No. e2867.
- (52) Afonin, K. A.; Danilov, E. O.; Novikova, I. V.; Leontis, N. B. TokenRNA: A new type of sequence-specific, label-free fluorescent biosensor for folded RNA molecules. *Chembiochem* 2008, *9*, 1902–1905.
- (53) Afonin, K. A.; Bindewald, E.; Yaghoubian, A. J.; Voss, N.; Jacovetty, E.; Shapiro, B. A.; Jaeger, L. In vitro assembly of cubic RNA-based scaffolds designed in silico. *Nat. Nanotechnol.* 2010, *5*, 676–682.
- (54) Afonin, K. A.; Viard, M.; Koyfman, A. Y.; Martins, A. N.; Kasprzak, W. K.; Panigaj, M.; Desai, R.; Santhanam, A.; Grabow, W. W.; Jaeger, L.; Heldman, E.; Reiser, J.; Chiu, W.; Freed, E. O.; Shapiro, B. A. Multifunctional RNA Nanoparticles. *Nano Lett.* 2014, 14, 5662–5671.
- (55) Sajja, S.; Chandler, M.; Striplin, C. D.; Afonin, K. A. Activation of Split RNA Aptamers: Experiments Demonstrating the Enzymatic Synthesis of Short RNAs and Their Assembly As Observed by Fluorescent Response. *J. Chem. Educ.* 2018, *95*, 1861–1866.
- (56) Autour, A.; C Y Jeng, S.; D Cawte, A.; Abdolahzadeh, A.; Galli, A.; Panchapakesan, S. S. S.; Rueda, D.; Ryckelynck, M.; Unrau, P. J. Fluorogenic RNA Mango aptamers for imaging small non-coding RNAs in mammalian cells. *Nat. Commun.* 2018, *9*, 656.
- (57) Chen, W.; Zhao, X.; Yang, N.; Li, X. Single mRNA Imaging with Fluorogenic RNA Aptamers and Small-molecule Fluorophores. *Angew Chem., Int. Ed.* 2022, *135*, No. e202209813.
- (58) Huang, Y.-H.; Trapp, V.; Puro, O.; Makinen, J. J.; Metsa-Ketela, M.; Wahl, M. C.; Belogurov, G. A. Fluorogenic RNA aptamers to probe transcription initiation and co-transcriptional RNA folding by multi-subunit RNA polymerases. *Methods Enzymol.* 2022, 675, 207–233
- (59) Mumbleau, M. M.; Meyer, M. R.; Hammond, M. C. Determination of In Vitro and Cellular Turn-on Kinetics for Fluorogenic RNA Aptamers. *J. Vis. Exp.* 2022, No. e64367.
- (60) Alam, K. K.; Tawiah, K. D.; Lichte, M. F.; Porciani, D.; Burke, D. H. A Fluorescent Split Aptamer for Visualizing RNA-RNA Assembly In Vivo. *ACS Synth. Biol.* 2017, *6*, 1710–1721.

- (61) Bui, M. N.; Brittany Johnson, M.; Viard, M.; Satterwhite, E.; Martins, A. N.; Li, Z.; Marriott, I.; Afonin, K. A.; Khisamutdinov, E. F. Versatile RNA tetra-U helix linking motif as a toolkit for nucleic acid nanotechnology. *Nanomedicine* 2017, *13*, 1137–1146.
- (62) Hong, E.; Halman, J. R.; Shah, A. B.; Khisamutdinov, E. F.; Dobrovolskaia, M. A.; Afonin, K. A. Structure and Composition Define Immunorecognition of Nucleic Acid Nanoparticles. *Nano Lett.* 2018, *18*, 4309–4321.
- (63) Srinivas, N.; Ouldridge, T. E.; Sulc, P.; Schaeffer, J. M.; Yurke, B.; Louis, A. A.; Doye, J. P.; Winfree, E. On the biophysics and kinetics of toehold-mediated DNA strand displacement. *Nucleic Acids Res.* 2013, *41*, 10641–10658.
- (64) Zadeh, J. N.; Steenberg, C. D.; Bois, J. S.; Wolfe, B. R.; Pierce, M. B.; Khan, A. R.; Dirks, R. M.; Pierce, N. A. NUPACK: Analysis and Design of Nucleic Acid Systems. *J. Comput. Chem.* 2011, *32*, 170–173
- (65) Lyubchenko, Y. L.; Shlyakhtenko, L. S. AFM for analysis of structure and dynamics of DNA and protein-DNA complexes. *Methods* 2009, *47*, 206–213.
- (66) Abraham, F. F.; Batra, I. P.; Ciraci, S. Effect of tip profile on atomic-force microscope images: A model study. *Phys. Rev. Lett.* 1988, 60, 1314–1317.
- (67) Vijayalakshmi, A.; Girish, V. Affordable image analysis using NIH Image/ImageJ. *Indian J. Cancer* 2004, 41, 47.
- (68) Zhang, D. Y.; Winfree, E. Control of DNA Strand Displacement Kinetics Using Toehold Exchange. *J. Am. Chem. Soc.* 2009, *131*, 17303–17314.
- (69) Khodakov, D. A.; Khodakova, A. S.; Linacre, A.; Ellis, A. V. Toehold-mediated nonenzymatic DNA strand displacement as a platform for DNA genotyping. *J. Am. Chem. Soc.* 2013, *135*, 5612–5619.
- (70) Afonin, K. A.; Kireeva, M.; Grabow, W. W.; Kashlev, M.; Jaeger, L.; Shapiro, B. A. Co-transcriptional assembly of chemically modified RNA nanoparticles functionalized with siRNAs. *Nano Lett.* 2012, *12*, 5192–5195
- (71) Yang, X.; Huang, J.; Wang, Q.; Wang, K.; Yang, L.; Huo, X. A one-step sensitive dynamic light scattering method for adenosine detection using split aptamer fragments. *Anal. Methods* 2011, *3*, 59–61
- (72) Jeng, S. C.; Chan, H. H.; Booy, E. P.; McKenna, S. A.; Unrau, P. J. Fluorophore ligand binding and complex stabilization of the RNA Mango and RNA Spinach aptamers. *RNA* 2016, *22*, 1884–1892
- (73) Zuker, M. Mfold web server for nucleic acid folding and hybridization prediction. *Nucleic Acids Res.* 2003, *31*, 3406–3415.
- (74) Shlyakhtenko, L. S.; Gall, A. A.; Lyubchenko, Y. L. Mica functionalization for imaging of DNA and protein-DNA complexes with atomic force microscopy. *Methods Mol. Biol.* 2013, *931*, 295–312